

RGBD Semantic Segmentation Using Spatio-Temporal Data-Driven Pooling

Yang He¹, Wei-Chen Chiu¹, Margret Keuper² and Mario Fritz¹

¹Max Planck Institute for Informatics ²University of Freiburg

Abstract. Beyond the success in classification, neural networks have recently shown strong results on pixel-wise prediction tasks like image semantic segmentation on RGBD data. However, the commonly used deconvolutional layers for upsampling intermediate representations to the full-resolution output still shows different failure modes, like imprecise segmentation boundaries and label mistakes particular on large, weakly textured objects (e.g. fridge, whiteboard, door). We attribute these errors in part to the rigid way, current network aggregate information, that can be either too local (missing context) or too global (inaccurate boundaries). Therefore we propose a data-driven pooling layer that integrates with fully convolutional architectures and utilizes boundary detection from RGBD image segmentation approaches. We extend our approach to leverage region-level correspondence across images with an additional temporal pooling stage. We evaluate our approach on the *NYU-Depth-V2* dataset comprised of indoor RGBD video sequences and make comparison with respect to various state-of-the-art baselines. We improve on the state-of-the-art and in particular in accuracy of the predicted boundaries and previously problematic classes.

1 Introduction

Consumer friendly and affordable combined image and depth-sensors such as *Kinect* are nowadays commercially deployed in scenarios such as gaming, personal 3D capture and robotic platforms. Towards understanding the semantic content of scenes captured in such data, there has been very active research on semantic image segmentation. In this task, the aim is to provide from a set of known classes a correct label for each pixel in the image plane. Semantic segmentation has broad applicability and achieved great progress in the past year in particular due to deep neural networks. Most recently, fully convolutional architectures [1] (FCN) have been proposed for this task, aiming at an end-to-end, joint learning from RGBD to semantic segmentations. Albeit its success in providing quality estimates of semantic labels on the coarse regions, it is at its core based on a rather rigid scheme with fixed rectangular pooling and upsampling operators, that lead to a fixed receptive field structure – invariant to the observed data. The consequences we have observed are twofold. On the one hand, the nature of the subsampling stages in its architecture can cause a loss of spatial resolution in the deep layers. The final predictions, computed from upsampling

low-resolution segmentations by the deconvolutional layers, apparently lack the details necessary for accurate boundary localization due to too coarse inference schemes (large receptive field). On the other hand, we have observed a weakness of such methods on larger, less structured areas that belong to label classes such as “clothes”, “curtain”, “book”, “whiteboard”. We hypothesize that for such classes this inference scheme is too fine grained (small receptive field) in order to get enough context for successful labeling.

This motivates us to propose a data-driven pooling scheme, allowing to leverage highly accurate non-semantic boundary information in CNN based semantic segmentation. In addition to leveraging spatial information, the proposed scheme facilitates pooling over time or varying viewpoints. For many scenarios of practical relevance such as robotics, an image sequence is naturally collected and provides a substantially richer source of information than a single image. With additional evidence from the images on the same scene recorded from a different view, we can get more information of the objects in an image, such as different viewpoints or scales. These cues potentially improve the accuracy of semantic segmentations.

The main contributions of our paper are:

- Instead of refining the boundaries in the semantic segmentation results of FCN posthoc by using CRF models [2] or learning semantic region similarity [3], we build on advances in RGBD image segmentation approaches [4] which already show accurate boundary detections and provide a guide for the inference. A data-driven pooling scheme is proposed that uses superpixels generated by RGBD image segmentation for defining the receptive field of pooled pixel-label predictions.
- Our scheme naturally extends to spatio-temporal pooling. The correspondence between the superpixels across frames is built using optical flow. Then, a pooling operator is proposed on the connected segments to generate the final segment labeling.
- Our proposed method is evaluated on the challenging semantic segmentation dataset *NYU-Depth-V2* and outperforms several baselines as well as the state of the art on the dataset. In particular, we improve on boundary precision and accuracy, as well as on difficult classes not well captured by other methods.

We organize the upcoming content of the paper as: In section 2, we first review the related work on convolutional networks based semantic segmentation, its extensions, and semantic segmentation based on multiple frames as observation. We elaborate our approach in section 3, and present the experimental results on *NYU-Depth-V2* [5] in section 4. Finally, this paper is concluded in section 5.

2 Related work

2.1 Fully convolutional networks and extensions:

Fully convolutional networks (FCN) [1] built on deep classification networks [6,7] carried their success forward to semantic segmentation networks that are also

end-to-end trainable. Benefiting from the end-to-end training, it uses raw pixels as input and computes hierarchical visual features from a pretrained model. Finally, the method upsamples the prediction by upsampling layers to directly generate dense predictions. Following the idea of FCN, there are several extensions. Chen *et al.* combines the strengths of conditional random field (CRF) and FCN to refine the prediction, thus achieving more favorable results. However, the key components in the work are not trained as a whole model. Zheng *et al.* designed an end-to-end trainable model based on FCN and CRF. They formulated the CRF model as a recurrent neural network (RNN), and integrate the CRF-RNN with convolutional networks. Noh *et al.* [8] showed that the FCN model has difficulties to extract small objects because the method only uses one deconvolution layer with large kernel size, which may ignore a lot of useful information. Thus they learned a multiple layer deconvolution network to up-sample the activations of fully convolutional networks to achieve more accurate and robust segmentations.

2.2 Boundary for Semantic Segmentation:

Boundary probabilities and edge detections have been exploited in many prior works on segmentation. Specifically, boundary information has recently been used in semantic segmentation by combining deep neural networks. Pooling areas can also be learnt [9], but then they are fixed and not data-dependent as when based on boundaries. Dai *et al.* [10] designed the convolutional feature masking layer for semantic segmentation, which allows networks to extract features in a stuff region with the help of superpixels. Gadde *et al.* [11] also improved the semantic segmentation using superpixel convolutional networks with bilateral inception, which can control to merge initial superpixels by parameters and generate different levels of regions. Chen *et al.* [12] proposed a network to predict task-specific edges and semantic segmentations simultaneously. This method is also built on the FCN model, and refines the output of the FCN by the estimated edges. In the above mentioned methods, segmentation is improved by using estimated edges or pre-computed superpixels. Both methods obviously showed the merit of providing boundary information to networks, which can then partition an image into several regions and generate more accurate segmentation. Our work follows a similar idea, but expresses the combination of boundaries and semantic segmentation as data-driven pooling strategy which still allows end to end training and a natural extension to spatio-temporal pooling.

2.3 Multi-view semantic segmentation:

The aim of multi-view semantic segmentation is to obtain better segmentations than such methods relying on single view information. How to leverage the information from multiple views and enforce temporal consistency is the key issue in multi-view semantic segmentation. Xiao *et al.* [13] built a markov random field model for the whole image sequence to improve the segmentation across different views. Floros *et al.* [14] enforced temporal consistency through an additional

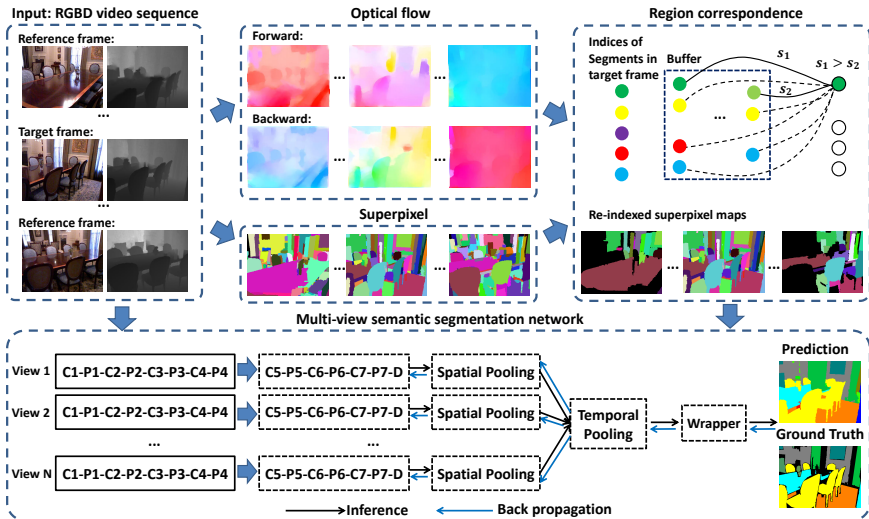


Fig. 1. Pipeline of our method. Our multi-view semantic segmentation network is built on the FCN (“C” refers to the convolution layer, “P” refers to the pooling layer, and “D” refers to the deconvolution layer), which fuse the information from multiple views with spatial-temporal data-driven pooling.

potential in conditional random fields by a 3D reconstruction model. Hermans *et al.* [15] also used the Bayesian update strategy to fuse the new classification results and a CRF model in 3D space to smooth the segmentation. Different to the above methods, we design an end-to-end trainable network which can introduce correspondences between multiple frames. Our end-to-end model allows us to train the whole model from raw pixels to the final segmentation, instead of training several parts separately.

3 Approach

In order to overcome the limitations of a fixed receptive field, we propose to leverage segmentations (not class specific) in a data-drive pooling scheme. Hereby, we draw on the rich body of work on image segmentation and combine it with recent deep learning approaches to semantic image segmentations with accurate boundaries and labels. Our approach naturally extends to image sequences in which we can employ spatio-temporal pooling for improved semantic segmentation performance.

3.1 Overview

Our method receives an image sequence as the input, and we are interested in providing the most accurate semantic segmentation of one view in the sequence, which we call *target frame*. Other frames are called *reference frames*. Generally, the target frame is located at an arbitrary position in the image sequence.

We leverage additional information from reference frames to improve the performance in the target frame. There are two main aspects in our system: region level correspondence and multi-view semantic segmentation network with data-driven pooling.

The pipeline of our method is summarized in Fig. 1. We first compute the superpixel segmentation of each frame and establish region level correspondence. Via the proposed data-drive pooling information is aggregated in a deep learning architecture that is imposed by the correspondence structure. Hereby, we achieve a tight integration of the superpixel segmentation into a deep learning framework that still allows for end-to-end training.

3.2 Region Level Correspondence

Mapping information from reference frames to the target frame is central to our framework. In order to establish the required correspondences, we pass the information frame by frame with optical flow across the video sequence. Ideally, precise pixel level correspondences could support the segmentation of the target frame. But, optical flow is not perfect and errors can easily accumulate in pixel level correspondences. Additionally, there are some regions in the target frame which might have been occluded in previous frames or will undergo occlusion in subsequent frames. Regions have proven to be effective in semantic segmentation [11,16,17], and they are more robust to the errors from optical flow than single pixels. [18]. Additionally, it is more efficient to reject entire regions in reference frames if we cannot find similar regions in the target frame than it would be to make these decisions on a pixel level.

Superpixels Therefore, we decide to establish correspondences on a superpixel level. To partition an image into several regions, we compute the superpixels [4] using RGBD images in each frame, and the optical flow between each pair of consecutive RGBD images. Epic flow [19] is an edge-perserving optical flow technique, which uses boundary probabilities as an input. To take advantage of the depth information, we utilize the RGBD version of the structured edge detection [20] to generate boundary estimates. Then Epic flow is computed in forward and backward directions.

Robust Spatio-Temporal Matching Since superpixels are not perfect either, an incorrect superpixel will cause the left of the sequence fail to match. To increase the possibility to match a region to the target frame, we save the superpixels of several previous frames to establish correspondences for each frame. For two regions from two different images, we use the intersection over union as the metric to determine whether these two region should be connected. Assuming R_c is the region in current frame to be matched, and R_p is a region already re-indexed as X in the past. We first flow the region R_c to R_p , and compute the intersection of union \overleftarrow{IoU}_{cp} . On the contrary, we can also compute $\overrightarrow{IoU}_{cp}$ by flowing from R_p to R_c . If $\min(\overleftarrow{IoU}_{cp}, \overrightarrow{IoU}_{cp}) > threshold_{sp}$, we will regard R_c

and R_p is a valuable matching pair. When R_c has several valuable matching pairs $R_{p_1}, R_{p_2}, \dots, R_{p_n}$ with segment indices $X_{p_1}, X_{p_2}, \dots, X_{p_n}$, and their matching scores are s_1, s_2, \dots, s_n , we assign R_c a new index X_{p_i} , where R_c and R_{p_i} has the highest matching score s_i . Applying such a matching procedure for all regions in the video, we can obtain a re-indexed superpixel map for each frame, which will be fed into the networks.

3.3 Multi-view Semantic Segmentation Network with Data-Driven Pooling

The power of CNN has been exploited in many computer vision tasks [6,21,22,23] by using pooling technique to extract holistic or localized features for whole images[6], or proposals[22]. While most of them extract feature in a rectangle region with fixed size, which fixes the aperture and therefore also the receptive fields. In addition, in order to aggregate the information from multiple views (the number of views varies for different regions), we need a flexible pooling strategy to train the whole model with multiple frames end-to-end. Thus we propose a data-driven pooling mechanism which extract high-level features guided by superpixels.

Data-Driven Pooling Our multi-view segmentation network is built on the fully convolutional network (FCN). We include a data-driven pooling layer after the last deconvolution layer, as shown in the bottom of Fig. 1. We transfer the pre-trained FCN-VGG16 to multi-view segmentation with region level correspondence. We only finetune the layers after *pool4* layer, as previous results have shown that they are quite stable [1]. Hence, we cache the output of the *pool4* layer, and retrain a networks taking *pool4* as input. This also turned out to be instrumental for training multi-view by conserving GPU memory.

We refine the output of deconvolution layer with superpixel and aggregate the information from multiple view by our proposed data-driven pooling, which can be decomposed into two steps: spatial pooling and temporal pooling. We can apply average pooling or max pooling to incorporate the superpixels. For max pooling, it maps the maximum number to output side, and redirects the gradient to input side. In this section, we take average pooling into an elaborate consideration, and formulate the forward and backward of the layer. The spatial pooling take an input feature map $I_s \in R^{N \times C \times H \times W}$, and generate the output $O_s \in R^{N \times C \times H \times W}$. Each channel of the frames is computed separately. It also needs a superpixel map $S \in R^{N \times H \times W}$ to guide the forward and backward part of the layer. Note that $\Omega_{ij} \in \{(x, y) | S(i, x, y) = j\}$ is a superpixel in i -th frame with segment index j , the forward of spatial average pooling can be formulated as

$$O_s(i, j, x_t, y_t) = \frac{1}{|\Omega_{ij}|} \sum_{(x_k, y_k) \in \Omega_{ij}} I_s(i, j, x_k, y_k), \quad (1)$$

where $(x_t, y_t) \in \Omega_{ij}$, thus the posteriors of all pixels in the j -th regions of i -th frame are enforced to be the same. In order to train our model, we

employ stochastic gradient descent for optimization. The gradient of the input $I(i, j, x_k, y_k)$, where $(x_k, y_k) \in \Omega_{ij}$, in spatial average pooling is calculated by back propagation [24],

$$\begin{aligned} \frac{\partial L}{\partial I_s(i, j, x_k, y_k)} &= \sum_{(x_t, y_t) \in \Omega_{ij}} \frac{\partial L}{\partial O_s(i, j, x_t, y_t)} \frac{\partial O_s(i, j, x_t, y_t)}{\partial I_s(i, j, x_k, y_k)} \\ &= \frac{1}{|\Omega_{ij}|} \sum_{(x_t, y_t) \in \Omega_{ij}} \frac{\partial L}{\partial O_s(i, j, x_t, y_t)}. \end{aligned} \quad (2)$$

Similarly, the temporal average pooling which fuse the information from multiple frames $I_t \in R^{N \times C \times H \times W}$ to one frame $O_t \in R^{C \times H \times W}$. Except superpixel map $S \in R^{N \times H \times W}$, it also needs a superpixel map on target frame $S_{target} \in R^{H \times W}$. Note that $\tilde{\Omega}_j \in \{(x, y) | S_{target}(x, y) = j\}$ is a superpixel with index j in target frame, The forward can be expressed as:

$$O_t(j, x_t, y_t) = \frac{1}{K} \sum_{i=1}^N \sum_{(x_k, y_k) \in \Omega_{ij}} \frac{1}{|\Omega_{ij}|} I_t(i, j, x_k, y_k), \quad (3)$$

where $(x_t, y_t) \in \tilde{\Omega}_j$, Ω_{ij} is the superpixel with index j of the i -th input frame, and $K = |\{\Omega_{ij} > 0 | 1 \leq i \leq N\}|$. The term $1/|\Omega_{ij}|$ is used to eliminate the affect of differences of region size. The gradient is calculated by

$$\begin{aligned} \frac{\partial L}{\partial I_t(i, j, x_k, y_k)} &= \sum_{(x_t, y_t) \in \tilde{\Omega}_j} \frac{\partial L}{\partial O_t(j, x_t, y_t)} \frac{\partial O_t(j, x_t, y_t)}{\partial I_t(i, j, x_k, y_k)} \\ &= \frac{1}{K|\Omega_{ij}|} \sum_{(x_t, y_t) \in \tilde{\Omega}_j} \frac{\partial L}{\partial O_t(j, x_t, y_t)}. \end{aligned} \quad (4)$$

Implementation Details We regard the frames which have groundtruth in a video as target frames. For each target frame, we collect up to 100 frames (Number of frames depends on the position of target frame in a video) around the target frame with step 3. As a result, we obtain 1449 video sequences with lengths varying from 28 to 101. Next, we compute the superpixel [4] and Epic flow [19] with default settings provided by their authors. The region correspondence is carried out with previous $K = 3$ frames, and $threshold_{sp} = 0.4$. Finally, we pick up 11 views for each sequence, which absolutely contain the target frame, as the input of our networks.

4 Experiments and Analysis

We evaluate and compare our method on *NYU-Depth-V2* [5] (NYUDv2) dataset. The NYUDv2 dataset contains 518 RGBD video sequences, which have more

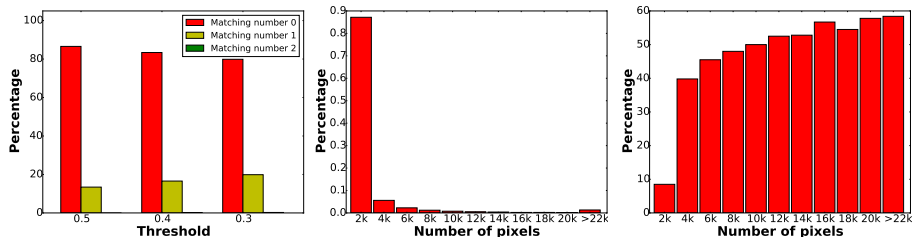


Fig. 2. Statistics on region correspondence. The left figure draws the histogram of successful matching number of regions between adjacent frames with different thresholds. The middle figure draws the histogram of region size. The right figure draws the histogram of matching number of regions in the whole video sequence.

than 400,000 image pairs. Among them, there are 1449 densely labeled frames, which are split into 795 training images and 654 testing images. We report the results on the labeled frame, using the same evaluation protocol and metrics as [1], pixel accuracy (*Pixel Acc.*), mean accuracy (*Mean Acc.*), region intersection over union (*Mean IoU*), and frequency weighted intersection over union (*f.w. IoU*).

4.1 Region Correspondence Analysis

As establishing good correspondences between reference and target frames is important in our method, we start with a study of the computed regions and their correspondences. We first make statistics on how many regions can be matched for a region in its neighboring frame as shown in Fig. 2 (left). We find that most of regions cannot find any matching region in other frame. In order to understand this phenomenon, we count the size of regions provided by superpixel in all 1449 labeled frames in Fig. 2 (middle). Besides, we count the number of matching regions on whole video of the segments in target frames, and get the distribution by the size of regions in Fig. 2 (right). This shows that most of the regions are small (less than 2000 pixels), and they are unlikely to find good matching regions. That is why there are almost 80% of the segments without correspondence. As a result, most successful regions are very large, which cover most area of the images, and they usually only have one match to its neighbor frame. Therefore, we decide to only consider the correspondence with the highest score for our data-driven pooling method which also reduces the computational complexity significantly.

4.2 Fine-tuning

We implement the proposed network using *Caffe* framework [25]. We use RGB images and HHA representations of depth and train the networks by stochastic gradient descent with momentum term. Due to the memory limitation and in line with previous studies, we first run FCN-VGG16 and cache the output *pool4_rgb*

Table 1. Comparison results of average and max data-driven spatio-temporal pooling.

Segment	Multi-View	Pixel Acc.	Mean Acc.	Mean IoU	f. w. IoU
AVERAGE	AVERAGE	70.1	53.8	40.1	55.7
AVERAGE	MAX	69.4	51.0	38.0	54.4
MAX	AVERAGE	66.4	45.4	33.8	49.6
MAX	MAX	64.9	44.5	32.1	47.9

Table 2. The performance of oracle case using groundtruth to label the regions.

Groundtruth	Pixel Acc.	Mean Acc.	Mean IoU	f. w. IoU
Current Frame	96.2	94.0	90.2	92.7
Next Frame	84.7	76.2	63.4	74.4

and *pool4_hha* and then finetune the layers after *pool4* with a new network which is the copy of higher layers in FCN. We use a minibatch size of 10, momentum 0.9, weight decay 0.0005 and fixed learning rate 10^{-14} . We finetune our model using cross entropy loss with 1000 iterations for all our models in the experiments, which decrease the training loss approximately from 2×10^5 to less than 10^5 .

4.3 Average vs. Max Data-Driven Spatio-Temporal Pooling

Our data-driven pooling aggregates the local information from multiple pixels within a segment and across multiple views. Average pooling and max pooling are canonical choices used in many deep neural network architectures that allow for end-to-end training. Here we test the average pooling and max pooling both in spatial and temporal pooling and show the results in Table 1. All the models are trained with multiple frames, and tested on multiple frames. Specifically, the first column specifies the spatial pooling type over the segment and the second column specifies the temporal pooling type across frames. Average pooling turns out to perform best for spatial and temporal pooling and therefore we use this combination in the rest of our experiments.

4.4 Oracle Performance using Groundtruth Labels

We perform two best-case analysis by computing an oracle performance where groundtruth labels are available for either reference or target frames. The first row of Table 2 shows the achievable performance by performing a majority vote of the groundtruth pixel labels on the employed superpixel from [4]. Thereby we achieve an upper bound of 96.2% on the pixel accuracy that is implied by the superpixel over-segmentation. In order to evaluate the effectiveness of our region correspondence, we use groundtruth labels of the next labeled frame in the sequence. We collect 143 views to conduct this experiment in NYUDv2, which have corresponding regions in next labeled frame. We ignore regions without correspondences in the next frame to compute the quantitative results, which are presented in Table 2. This best-case analysis for correspondences results in a



Fig. 3. Example of groundtruth limitation and segmentation results of oracle case. Row 3 and 2 draw color images of target frame and next labeled frame, respectively. And row 4 and 1 draw their groundtruth. The segmentation result with groundtruth of target frame is shown in row 5, and the result with groundtruth of next frame is shown in row 6. We point out the regions in different frames with white bounding box, which are the same object of different views but labeled as different classes.

pixel accuracy of 84.7%. Both oracle performances indicate a strong potential for performance improvements in our setup in all 4 reported measures. In addition, the lower two rows in Fig. 3 show examples labeling for the best-case study.

4.5 Groundtruth Analysis

At a closer look, it turns out that at least part of the performance loss in the best-case analysis for the correspondences is not to be attributed to bad matches between regions. In Fig. 3, we display some of the limitation of the annotations. In several cases, as the ones shown in the figure, the labeling is inconsistent and objects change label during the sequence. From left to right in Fig. 3, table changes to desk, table changes to dresser, floor changes to floor mat, bookshelf changes to shelves, cabinet changes to other-furniture, and window changes to blinds. Consequently, we see mistakes in the last two rows corresponding to the best case results due to inconsistent labelings.

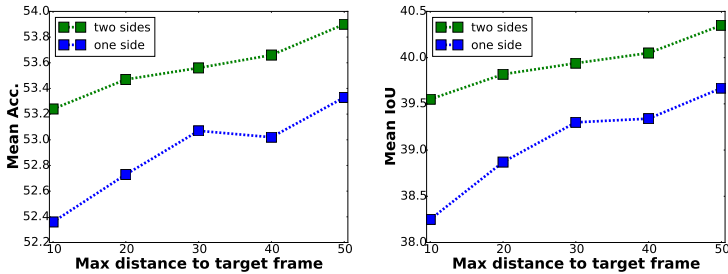


Fig. 4. The performance of multi-view prediction with different max distance. Green lines show the results of using the views in the future and past. Blue lines show the results of only using the past views.

Table 3. Comparison results with baselines on NYUDv2

Methods	Pixel Acc.	Mean Acc.	Mean IoU	f. w. IoU
FCN [1]	65.4	46.1	34.0	49.5
Multi-view Pixel Network	66.2	45.9	34.6	50.2
Single-view Superpixel Network	68.5	48.7	36.0	52.9
Our full model	70.1	53.8	40.1	55.7

4.6 Analysis of Multi-View Prediction

In our multi-view model, we subsample frames from the whole video for computational considerations. There is a trade-off between close-by and distant frames to be made. If we select frames far away from the target frames, they can provide more diverse views of an object, while matching is more challenging and potentially less accurate than for close-by frames. Hence, we analyze the influence of the distance of selected frames to target frames, and report the *Mean Acc.* and *Mean IoU* in Fig 4. As a result, providing wider views is helpful, as the performance is improved with the increasing of max distance. And selecting the data in the future, which is another way to provide wider views, also contributes to the improvements of performance.

4.7 Comparison to Baseline Methods

We compare to three baselines: fully convolutional networks (FCN) [1], multi-view pixel-level correspondence network, and single-view spatial pooling network. The second baseline and the third baseline are built on the top of FCN-VGG16. These baselines aim at analyzing the performance of the three key ingredients that we are building on: FCN, flow, superpixels. The quantitative comparison is listed in Table 3.

The second baseline, multi-view pixel-level correspondence network (Multi-view Pixel Network) uses the per-pixel correspondence by Epic flow, and applies average pooling to fuse the information from multiple view. Table 3 shows that

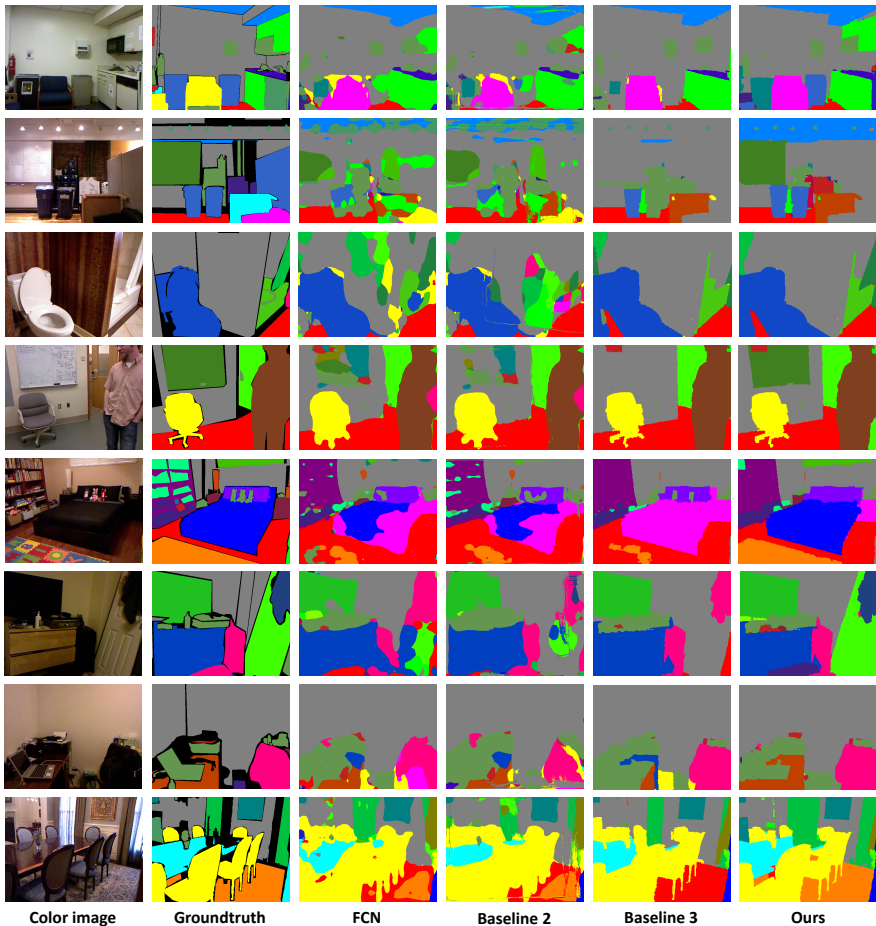


Fig. 5. Visualization examples of semantic segmentation on NYUDv2. Column 1 shows the RGB images and column 2 shows the ground truth (black represents the unlabeled pixels). column 3 shows the results from FCN [1], column 4 and 5 shows the results from the second baseline and the third baseline, and the results from our whole system are shown in the column 6. Best view in color.

baseline 2 has already better performance than FCN in 3 out of 4 measures, which means leveraging multiple views benefits the estimation of a single pixel. But the optical flow is not perfect, thus obtaining accurate pixel-level correspondence is challenging. Consequently, the full model, which is built on the region-level correspondence, has a significant improvement over this baseline and FCN in all 4 measures.

The third baseline introduces superpixel to the network (Single-view Superpixel Network), and we train and test it using only one view. The data-driven pooling scheme divides the FCN prediction into several segments and refines

the prediction by enforcing the pixels in a segment having the same posterior. For each segment, we apply average pooling to extract the representation of the segments. Comparing baseline 3 with FCN, we observe a performance improvement on all four metrics of at least 2 percentage points (pp), which clearly shows the effectiveness of combining superpixel with convolutional networks. Our full model consistently improves over all baselines and outperforms the FCN model $4.7pp$, $7.7pp$, $6.1pp$, $6.2pp$.

Besides, we also report the qualitative results as shown in Fig 5. Our data-driven pooling networks can generate more precise and smooth segmentation than FCN and multi-view networks with pixel correspondence. And it also achieves more accurate estimation than single-view model. Therefore, leveraging multi-view data and using data-driven pooling to integrate the spatial-temporal information are effective.

4.8 Analysis of Semantic Segmentation Boundary Accuracy

In order to quantify the improvement on semantic boundary localization based on the proposed data-driven pooling scheme, we use Boundary Precision Recall (BPR), as also used in image or video segmentation benchmark [26,27] for evaluation. Fig 6 shows the resulting semantic boundary average precision-recall curve. We conclude that our method generates more accurate boundaries than FCN, which achieve 0.477 BPR score while our method achieves 0.647. Besides, our method even improves on the superpixel [4] we build on, which means our method can successfully merge over-segmentations or non-semantic boundaries between adjacent instances of the same semantic class.

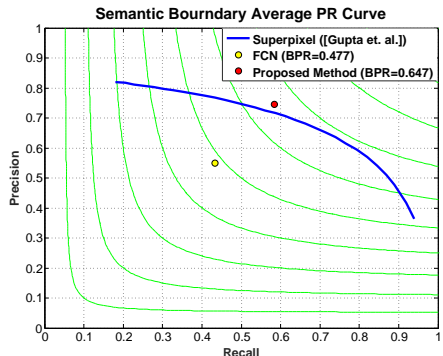


Fig. 6. Precision-recall curve on semantic boundaries on the NYUDv2 dataset.

4.9 Comparison with State-of-the-Art

We evaluate and analyze our final results on the NYUDv2 40 class semantic segmentation and compare our method to state-of-the-art methods [1,4,28,29,17]. The quantitative results are shown in Table 4 ¹. The multi-view model (Multi-View) leverages multiple views by from unlabeled data in NYUDv2, and we

¹ For [1], overall performance is obtained from the respective paper and report the performance of 40 class were computed with the authors' code.

Table 4. Performance on the 40 class semantic segmentation task. We compare our method with five state-of-the-art methods: [1,4,28,29] are also based on convolutional networks, and [17] is region labeling method, which is also related to ours. We mark the best performance in all methods with **BOLD** font, and the second best one is written with UNDERLINE.

	wall	floor	cabinet	bed	chair	sofa	table	door	window	bookshelf	picture	counter	blinds	desk	shelves
Long <i>et al.</i> [1]	69.9	79.4	50.3	66.0	47.5	53.2	32.8	22.1	39.0	36.1	50.5	54.2	45.8	11.9	8.6
Gupta <i>et al.</i> [4]	68.0	81.3	44.9	65.0	47.9	47.9	29.9	20.3	32.6	18.1	40.3	51.3	42.0	11.3	3.5
Kendall <i>et al.</i> [28]	-	-	-	-	-	-	-	-	-	-	-	-	-	-	-
Eigen <i>et al.</i> [29]	-	-	-	-	-	-	-	-	-	-	-	-	-	-	-
Deng <i>et al.</i> [17]	65.6	79.2	51.9	66.7	41.0	55.7	36.5	20.3	33.2	32.6	44.6	53.6	<u>49.1</u>	10.8	<u>9.1</u>
Ours (Single-View)	<u>72.4</u>	<u>84.3</u>	<u>52.0</u>	<u>71.5</u>	<u>54.3</u>	<u>58.8</u>	<u>37.9</u>	<u>28.2</u>	<u>41.9</u>	<u>38.5</u>	<u>52.3</u>	<u>58.2</u>	49.7	14.3	8.1
Ours (Multi-View)	72.7	85.7	55.4	73.6	58.5	60.1	42.7	30.2	42.1	41.9	52.9	59.7	46.7	<u>13.5</u>	9.4

	curtain	dresser	pillow	mirror	floormat	clothes	ceiling	books	fridge	tv	paper	towel	showercurtain	box	whiteboard
Long <i>et al.</i> [1]	32.5	31.0	37.5	22.4	13.6	18.3	<u>59.1</u>	27.3	27.0	41.9	15.9	26.1	14.1	<u>6.5</u>	12.9
Gupta <i>et al.</i> [4]	29.1	34.8	34.4	16.4	28.0	4.7	60.5	6.4	14.5	31.0	14.3	16.3	4.2	2.1	14.2
Kendall <i>et al.</i> [28]	-	-	-	-	-	-	-	-	-	-	-	-	-	-	-
Eigen <i>et al.</i> [29]	-	-	-	-	-	-	-	-	-	-	-	-	-	-	-
Deng <i>et al.</i> [17]	47.6	27.6	42.5	<u>30.2</u>	<u>32.7</u>	12.6	56.7	8.9	21.6	19.2	28.0	28.6	22.9	1.6	1.0
Ours (Single-View)	<u>42.9</u>	<u>35.9</u>	40.8	<u>27.7</u>	31.9	<u>19.3</u>	55.6	<u>28.2</u>	<u>38.3</u>	<u>46.9</u>	17.6	<u>31.2</u>	11.0	<u>6.5</u>	<u>28.2</u>
Ours (Multi-View)	40.7	44.1	<u>42.0</u>	34.5	35.6	22.2	55.9	29.8	41.7	52.5	<u>21.1</u>	34.4	<u>15.5</u>	7.8	29.2

	person	nightstand	toilet	sink	lamp	bath tub	bag	other struct	other furni	other props	Pixel Acc.	Mean Acc.	Mean IoU	f. w. IoU
Long <i>et al.</i> [1]	57.6	30.1	61.3	44.8	32.1	39.2	4.8	15.2	7.7	<u>30.0</u>	65.4	46.1	34.0	49.5
Gupta <i>et al.</i> [4]	0.2	27.2	55.1	37.5	34.8	<u>38.2</u>	0.2	7.1	6.1	23.1	60.3	-	28.6	47.0
Kendall <i>et al.</i> [28]	-	-	-	-	-	-	-	-	-	-	68.0	45.8	32.4	-
Eigen <i>et al.</i> [29]	-	-	-	-	-	-	-	-	-	-	65.6	45.1	34.1	51.4
Deng <i>et al.</i> [17]	9.6	30.6	48.4	41.8	28.1	27.6	0	9.8	7.6	24.5	63.8	-	31.5	48.5
Ours (Single-View)	66.7	<u>34.1</u>	62.8	47.8	<u>35.1</u>	26.4	8.8	19.3	<u>10.9</u>	29.2	<u>68.4</u>	<u>52.1</u>	<u>38.1</u>	<u>54.0</u>
Ours (Multi-View)	60.7	42.2	<u>62.7</u>	<u>47.4</u>	38.6	28.5	<u>7.3</u>	<u>18.8</u>	15.1	31.4	70.1	53.8	40.1	55.7

also test our single-view model (Single-View) that is tested on single frames. Already our single view results – which only use additional data at training time – are better than the state of the art performance in all 4 metrics by *2.9pp*, *6.0pp*, *4.0pp*, *2.6pp* respectively. Our multi-view model achieves a consistent improvement over the single view model and outperform all competitors in all four metrics by *2.1pp*, *7.7pp*, *6.0pp*, *4.3pp* respectively. Particular strong improvements are observed on challenging objects such as whiteboard, bag, other furniture where we roughly double the performance. In particular, the substantial improvement on the class averaged accuracy is encouraging as here no particular fitting to single classes or large classes is observed. Fig. 5 shows example segmentations obtained by our multi-view model, that shows accurate boundaries (e.g. chair legs), consistent labeling of large objects (e.g. bed, whiteboard, door) and small objects (e.g. ceiling lights).

5 Conclusion

In this paper, we have presented a novel semantic segmentation approach with using image sequences. We design a multi-view semantic segmentation network with data-driven spatio-temporal pooling which can receive multiple images and their correspondence as input. We propagate the information from multiple views to the target frame, and significantly improve the semantic segmentation performance on the target frame. Besides, our method can leverage large scale unlabeled images for training, and we show that using additional data also benefits single image semantic segmentation.

References

1. Long, J., Shelhamer, E., Darrell, T.: Fully convolutional networks for semantic segmentation. In: CVPR. (2015)
2. Chen, L.C., Papandreou, G., Kokkinos, I., Murphy, K., Yuille, A.L.: Semantic image segmentation with deep convolutional nets and fully connected crfs. In: ICLR. (2014)
3. Harley, A.W., Derpanis, K.G., Kokkinos, I.: Learning dense convolutional embeddings for semantic segmentation. In: ICLR Workshop. (2015)
4. Gupta, S., Girshick, R., Arbeláez, P., Malik, J.: Learning rich features from rgb-d images for object detection and segmentation. In: ECCV. (2014)
5. Nathan Silberman, Derek Hoiem, P.K., Fergus, R.: Indoor segmentation and support inference from rgb-d images. In: ECCV. (2012)
6. Krizhevsky, A., Sutskever, I., Hinton, G.E.: Imagenet classification with deep convolutional neural networks. In: NIPS. (2012)
7. Simonyan, K., Zisserman, A.: Very deep convolutional networks for large-scale image recognition. In: ICLR. (2015)
8. Noh, H., Hong, S., Han, B.: Learning deconvolution network for semantic segmentation. In: ICCV. (2015)
9. Malinowski, M., Fritz, M.: Learning smooth pooling regions for visual recognition. In: 24th British Machine Vision Conference, (BMVC). (2013)
10. Dai, J., He, K., Sun, J.: Convolutional feature masking for joint object and stuff segmentation. In: CVPR. (2015)
11. Gadde, R., Jampani, V., Kiefel, M., V. Gehler, P.: Superpixel convolutional networks using bilateral inceptions. arXiv preprint arXiv:1511.06739 (2015)
12. Chen, L.C., Barron, J.T., Papandreou, G., Murphy, K., Yuille, A.L.: Semantic image segmentation with task-specific edge detection using cnns and a discriminatively trained domain transform. arXiv preprint arXiv:1511.03328 (2015)
13. Xiao, J., Quan, L.: Multiple view semantic segmentation for street view images. In: CVPR. (2009)
14. Floros, G., Leibe, B.: Joint 2d-3d temporally consistent semantic segmentation of street scenes. In: CVPR. (2012)
15. Hermans, A., Floros, G., Leibe, B.: Dense 3d semantic mapping of indoor scenes from rgb-d images. In: ICRA. (2014)

16. Arbeláez, P., Hariharan, B., Gu, C., Gupta, S., Bourdev, L., Malik, J.: Semantic segmentation using regions and parts. In: CVPR. (2012)
17. Deng, Z., Todorovic, S., Jan Latecki, L.: Semantic segmentation of rgb-d images with mutex constraints. In: CVPR. (2015)
18. Brox, T., Malik, J.: Large displacement optical flow: descriptor matching in variational motion estimation. TPAMI (2011)
19. Revaud, J., Weinzaepfel, P., Harchaoui, Z., Schmid, C.: Epicflow: Edge-preserving interpolation of correspondences for optical flow. In: CVPR. (2015)
20. Dollár, P., Zitnick, C.: Structured forests for fast edge detection. In: CVPR. (2013)
21. Sermanet, P., Eigen, D., Zhang, X., Mathieu, M., Fergus, R., LeCun, Y.: Overfeat: Integrated recognition, localization and detection using convolutional networks. arXiv preprint arXiv:1312.6229 (2013)
22. Girshick, R.: Fast r-cnn. In: CVPR. (2015)
23. He, K., Zhang, X., Ren, S., Sun, J.: Spatial pyramid pooling in deep convolutional networks for visual recognition. TPAMI (2015)
24. Rumelhart, D.E., Hinton, G.E., Williams, R.J.: Learning representations by back-propagating errors. *Cognitive modeling* 5(3) (1988) 1
25. Jia, Y., Shelhamer, E., Donahue, J., Karayev, S., Long, J., Girshick, R., Guadarrama, S., Darrell, T.: Caffe: Convolutional architecture for fast feature embedding. In: Proceedings of the ACM International Conference on Multimedia. (2014)
26. Galasso, F., Nagaraja, N.S., Cardenas, T.J., Brox, T., Schiele, B.: A unified video segmentation benchmark: Annotation, metrics and analysis. In: ICCV. (2013)
27. Arbelaez, P., Maire, M., Fowlkes, C., Malik, J.: Contour detection and hierarchical image segmentation. TPAMI (2011)
28. Kendall, A., Vijay, B., Cipolla, R.: Bayesian segnet: Model uncertainty in deep convolutional encoder-decoder architectures for scene understanding. arXiv preprint arXiv:1511.02680 (2015)
29. Eigen, D., Fergus, R.: Predicting depth, surface normals and semantic labels with a common multi-scale convolutional architecture. In: ICCV. (2015)